Proceedings of the Combustion Institute, Volume 28, 2000/pp. 2785–2792

EFFECTS OF FINITE SAMPLE WIDTH ON TRANSITION AND FLAME SPREAD IN MICROGRAVITY

W. E. MELL[1] AND T. KASHIWAGI[2]
[1]*Mechanical Engineering Department*
University of Utah
Salt Lake City, UT 84112-1109, USA
[2]*National Institute of Standards and Technology*
Building and Fire Research Laboratory
Gaithersburg, MD 20899-8652, USA

In most microgravity studies of flame spread, the flame is assumed to be two-dimensional, and two-dimensional models are used to aid data interpretation. However, since limited space is available in microgravity facilities, the flames are limited in size. It is important, therefore, to investigate the significance of three-dimensional effects. Three-dimensional and two-dimensional simulations of ignition and subsequent transition to flame spread were performed on a thermally thin cellulosic sample. Ignition occurred by applying a radiant heat flux in a strip across the center of the sample. The sample was bounded by an inert sample holder. Heat loss effects at the interface of the sample and the sample holder were tested by varying the thermal-physical properties of the sample holder. Simulations were also conducted with samples of different widths and with different ambient wind speeds (i.e., different levels of oxygen supply).

The width of the sample affected both the duration of the flame transition period and the post-transition flame spread rate. Finite width effects were most significant when the ambient wind was relatively small (limited oxygen supply). In such environments, the velocity due to thermal expansion reduced the net inflow of oxygen enough to significantly affect flame behavior. For a given sample width, the influence of thermal expansion on the net incoming oxygen supply decreased as the ambient wind speed increased. Thus, both the transition and flame spread behavior of the three-dimensional flame (along the centerline) tended to that of the two-dimensional flame with increasing ambient wind speed. Heat losses to the sample holder were found to affect the flame spread rate in the case of the narrowest sample with the slowest ambient wind.

Introduction

Many flame spread studies over a solid fuel surface in microgravity have been conducted with the motivation of improving our understanding of the physics relevant to fire safety in a spacecraft. Almost all these studies were intended to observe the flame spread behavior in a two-dimensional configuration, and the results were compared with calculated data based on two-dimensional models. However, by necessity, these experiments were generally conducted in spatially limited experimental volumes which resulted in relatively narrow samples despite the original intention of a two-dimensional experimental configuration. For example, a majority of experimental studies were conducted with 5 cm width samples [1–3], but others were with 3 cm width [4] and 6.35 mm width samples [5]. Future microgravity combustion experiments in space will be carried out mainly on the international space station (ISS), either in a dedicated combustion integrated rack (CIR) with specific inserts for a given experiment or in the microgravity science glovebox. Drop towers, sounding rockets, and airplanes will continue to be used for ground-based experiments. The available test chamber volume of these facilities will be limited, and future flame spread experiments will be restricted to using relatively narrow samples. It is, therefore, critically important to determine whether these sample widths will produce truly two-dimensional flame behavior. Three-dimensional effects on flame spread along a sample which is too narrow can, for example, arise from enhanced oxygen supply from the outer free stream and from heat loss to a sample holder. In this paper, transient two-dimensional and three-dimensional simulation codes [6] were used to investigate the effects of finite sample width on flame behavior. These codes simulate the development of flame spread from ignition, through transition to established flame spread.

Theoretical Model

Since the theoretical model used for the condensed phase sample has been described in Ref. [7],

Report Documentation Page

Form Approved
OMB No. 0704-0188

1. REPORT DATE	2. REPORT TYPE	3. DATES COVERED
04 AUG 2000	**N/A**	**-**

4. TITLE AND SUBTITLE	5a. CONTRACT NUMBER
Effects of Finite Sample Width on Transition and Flame Spread in Microgravity	5b. GRANT NUMBER
	5c. PROGRAM ELEMENT NUMBER
6. AUTHOR(S)	5d. PROJECT NUMBER
	5e. TASK NUMBER
	5f. WORK UNIT NUMBER
7. PERFORMING ORGANIZATION NAME(S) AND ADDRESS(ES) **Mechanical Engineering Department University of Utah Salt Lake City, UT 84112-1109, USA**	8. PERFORMING ORGANIZATION REPORT NUMBER
9. SPONSORING/MONITORING AGENCY NAME(S) AND ADDRESS(ES)	10. SPONSOR/MONITOR'S ACRONYM(S)
	11. SPONSOR/MONITOR'S REPORT NUMBER(S)

12. DISTRIBUTION/AVAILABILITY STATEMENT
Approved for public release, distribution unlimited

13. SUPPLEMENTARY NOTES
See also ADM001790, Proceedings of the Combustion Institute, Volume 28. Held in Edinburgh, Scotland on 30 July-4 August 2000., The original document contains color images.

14. ABSTRACT

15. SUBJECT TERMS

16. SECURITY CLASSIFICATION OF:			17. LIMITATION OF ABSTRACT	18. NUMBER OF PAGES	19a. NAME OF RESPONSIBLE PERSON
a. REPORT	b. ABSTRACT	c. THIS PAGE			
unclassified	**unclassified**	**unclassified**	**UU**	**8**	

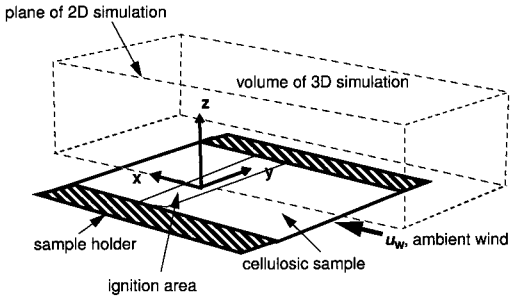

FIG. 1. Schematic showing the cellulosic sample and computational domains of the two- and three-dimensional simulations. The two-dimensional simulation domain was the $y = 0$ plane. A characteristic char pattern from the radiative ignition source is also shown. A sample holder abutted the cellulosic sample on the y boundaries. By changing the thermal–physical properties of the sample holder, the influence of heat loss to the sample holder on flame behavior was tested.

only a summary will be given here. A global approach is used to define both the gas-phase oxidation reaction and the thermal degradation reactions of the condensed phase. Although more detailed kinetic modeling is possible, the numerical solution of the resulting system of equations would be prohibitively expensive. The thermal degradation of the cellulosic sample is modeled by three exothermic global reactions governing pyrolysis (slightly exothermic), thermal oxidation, and char oxidation. The evolution of the thermal degradation process is governed by conservation equations for solid mass, cellulose, char, and energy with Arrhenius-type reaction rates [8]. The global kinetic constants and heats of reaction were obtained by thermogravimetric analysis and are identical to those used in Refs. [6,9]. As reported in Ref. [3], the sample's thickness is 0.13 mm, area density is 5.7 mg/cm^2, specific heat is 0.96 J/(g · K), and the emissitivity is 0.6. The specific heat increases linearly with temperature and is also used for the char and cellulose. The sample is assumed to be thermally thin and of uniform composition with depth.

Radiative losses from the surface are included. It has not been demonstrated that radiative heat transfer has a significant effect on flames over thermally thin fuels which are not near extinction. This regime is the focus of our paper. For example, Altenkirch et al. [5] have found that for thermally thin fuels, heat transfer to the fuel surface drives the flame spread and is dominated by conduction. Furthermore, as the sample width increases, the shape factor between the flame and the fuel surface ahead of the flame will reach its value for a two-dimensional flame, implying that the radiative flux to the surface will asymptote to its value for a two-dimensional flame. As will be seen below, this is consistent with the trend of both the spread rate and the duration of the transition period with increasing sample width. Thus, it is unlikely that including thermal radiation in the gas phase will change the findings of the paper.

The gas-phase model [8] consists of the conservation equations for total mass, momentum (full Navier–Stokes), energy, and species mass fractions (fuel and oxygen) formulated in the low Mach number limit. A global one-step reaction

$$[\text{fuel gas}] + \nu_{O_2}\,[\text{oxygen}] \rightarrow \text{product} \qquad (1)$$

with an Arrhenius rate is used. The pre-exponential factor in the reaction rate is 5.0×10^9 cm^3/(g s), the activation energy is 67 kJ/mol, the heat of combustion is 35 kJ/g, and the stoichiometric constant is $\nu_{O_2} = 3.57$. These values are identical to those used in previous two-dimensional [3] and three-dimensional [6,9] studies. The average molecular weight is assumed to be constant; temperature-dependent molecular transport coefficients are used. All gases have equal mass diffusivity which is not necessarily equal to the thermal diffusivity. Ignition is initiated by an external radiative flux on the sample surface.

Numerical Model

Both two- and three-dimensional simulations were performed. A sketch of the cellulosic sample and the two- and three-dimensional simulation domains are shown in Fig. 1. The domain for the two-dimensional simulations consists of the $y = 0$ (centerline) plane. The governing equations for the condensed phase are solved using a stiff ordinary differential equation solver. A finite difference control volume approach on a staggered grid is used to solve the gas-phase equations. A time-splitting algorithm is used for the species and temperature equations since the characteristic time scale of the chemical reaction is relatively small compared to that for diffusion and convection (high Damköhler number) [8]. This method involves first solving the species and temperature equations without the convective and diffusive terms using a stiff ordinary differential equation solver over small time steps. The global time stepping is performed using an alternating direction implicit scheme on the convective and diffusive terms. The momentum equation is solved using a projection method; the solution to the Poisson equation for the pressure perturbation is found with a direct solver.

There were two assumed symmetry planes in the three-dimensional simulations. One parallel to the plane of the sample and passing through its middle; the other was perpendicular to the plane of the sample, passing through the centerline of the sample in a direction parallel to the ambient wind (see Fig. 1).

Thus, in the three-dimensional calculations, one-quarter of a corresponding experimental volume was simulated. The physical dimensions of the three-dimensional computational domain were 12:8 × 6.4 × 4.8 cm in the x, y, and z directions, respectively (12.8 × 4.8 cm for two-dimensions); the overall sample size in the three-dimensional simulations was no larger than 10 cm long × 4.5 cm wide. Note that taking into account the symmetry assumptions, this corresponds to simulating flame spread on a 10 cm long × 9 cm wide sample.

The numerical grid was uniform in the horizontal directions and stretched in the vertical. Cell sizes were 0.66 mm in the horizontal directions (parallel to the sample); they start at 0.25 mm at the sample surface and stretch to 2 mm at the top of the computational domain. Various grid resolutions were used to ensure grid independence of the results (e.g., flame spread rates, quenching conditions). A typical three-dimensional grid contained about 600,000 grid points (192 × 96 × 32). For the three-dimensional runs, approximately 14 h CPU time are needed for 1 s of simulated real time on current-generation workstations.

The radiative flux on the sample ramped up in time following $\tanh[t/(0.75\ \mathrm{s})]$; at $t = 3.5$ s it was turned off. This procedure is consistent with previous simulation [3,6] and experimental studies [9]. This flux decayed exponentially with distance from the $x = 0$ as $\exp[-(x/h)^2]$. The half-width profile $h = 0.25$ cm. Convective oxygen supply to the flame was controlled by varying the magnitude of the ambient wind u_w which was composed of 33% oxygen ($Y_O = 0.33$). With $Y_O = 0.33$, the ambient wind speed corresponding to an oxygen-limited regime was known from the authors' previous work [6].

Zero gradient conditions are used for the farfield boundary values of the mass fractions and temperature which decay exponentially with distance from the flame. This is not appropriate for the velocity field which decays quadratically [8]. Instead, boundary conditions were obtained from an analytically determined velocity potential. Following Ref. [8], the velocity on a computational boundary, $\underline{u}_{bc}$, is

$$\underline{u}_{bc} = \underline{u}_e + \underline{u}_W = \nabla\Phi + \underline{u}_W,$$
$$\rho_\infty h_\infty \nabla^2\Phi = \dot{q} \qquad (2)$$

Here, $\underline{u}_e = (u_e, v_e, w_e)$ is the expansion velocity vector, $\underline{u}_w = (u_w, 0, 0)$ is the ambient wind velocity vector (see Fig. 1), Φ is the remainder potential, q is the volumetric heat release rate of combustion, are ρ_∞ and h_∞ are the ambient density and enthalpy. The solution for Φ, over the semi-infinite domain ($z > 0$) can be calculated using a Green's function, $G(x, y, z; x', y', z')$,

$$\Phi(x, y, z, t) = \int_{-\infty}^{\infty}\int_{-\infty}^{\infty}\int_{0}^{\infty} \nabla^2\Phi\ G dx'dy'dz' + \int_{-\infty}^{\infty}\int_{-\infty}^{\infty} \frac{\partial\Phi(x', y', 0)}{\partial z}\ G\ dx'dy' \qquad (3)$$

where on the sample surface

$$\rho_\infty h_\infty \frac{\partial\Phi(x, y, 0)}{\partial z} = h\dot{m}_l'' - k\frac{\partial T}{\partial z} \qquad (4)$$

Here, $\dot{m}''$ is the total mass flux from the sample, and k is the thermal conductivity. Thus, Φ and, therefore $\underline{u}_{bc}$ depend on the mass flux and heat transfer at the sample surface and on the chemical heat released by the gas-phase reactions. The domain is open to the ambient environment, which results in a constant thermodynamic pressure. Note that in an experimental study, enclosure effects may be present which are not accounted for in the simulation.

Results and Discussion

The effects of a finite sample width on flame behavior were investigated by simulating samples of three different widths: 2 cm, 4 cm, and 9 cm. To ensure that there were no confounding factors related to numerical boundary conditions, the size of the computational domain was kept the same for all cases. In experimental studies [9], the cellulosic sample is held in place by a 0.5 mm thick, American Iron and Steel Institute (AISI) 304, stainless steel holder. Most of the three-dimensional simulations, therefore, had the cellulosic sample bordered by a solid with the thermal–physical properties of AISI 304 stainless steel (see Fig. 1). In order to test the effects of heat loss to a steel sample holder, additional simulations were run with a sample holder which had the thermal-physical properties of the sample (but was inert).

This paper focuses on the effects of a finite width sample on flame behavior during two different regimes: the transition period between localized ignition and flame spread and the posttransition period of established, possibly steady-state, flame spread. To survive transition, a sufficient amount of oxygen must reach the reaction zone. In these simulations ($Y_O = 0.33$), the oxygen supplied by an ambient wind of $u_w \approx 1.5$ cm/s or below was insufficient for the flame to survive transition [6]. Three different ambient wind conditions were used, $u_w = 2$ cm/s, 5 cm/s, 10 cm/s. When $u_w = 2$ cm/s, flame transition and spread occurs in an oxygen-limited environment. In this case, the flame is expected to be relatively weak and, therefore, more sensitive to changes in its environment (such as heat losses to a steel versus a paper sample holder). As u_w increases from 2 cm/s, the oxygen supply improves and the flame becomes more robust. At u_w values larger than those

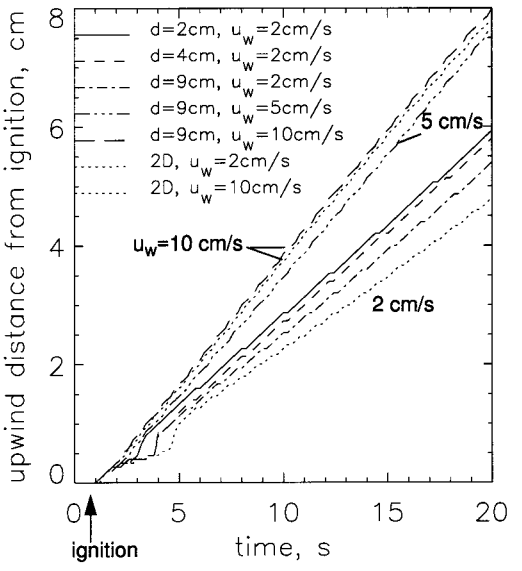

FIG. 2. Flame location along the centerline versus time for all three-dimensional cases with a stainless steel holder (no cases with a paper holder are shown). Two two-dimensional cases are also shown, both as dotted lines. The step-like behavior seen on the curves is not physical, but a consequence of solving the discretized equations.

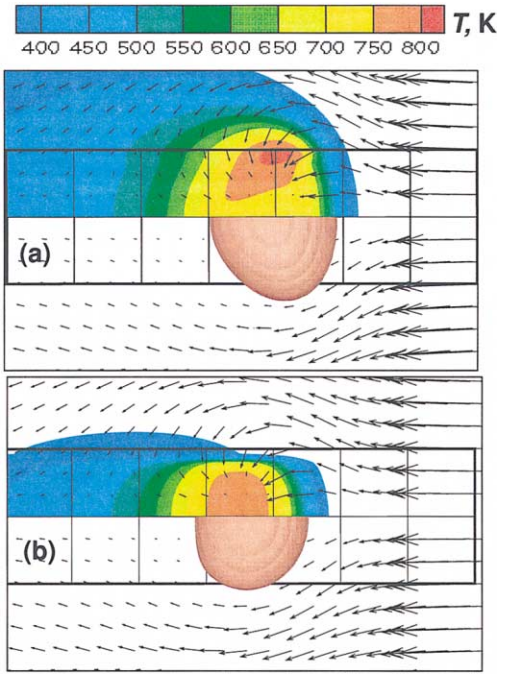

FIG. 3. Top view of flame shape, convective (on bottom half of each figure) and net (on top half of each figure) oxygen mass flux vectors, and color contours of the sample temperature are shown for the $u_w = 2$ cm/s, 2 cm wide sample. (a) Paper sample holder. (b) Steel sample holder. The mass flux vectors are in a horizontal plane at $z = 2.5$ mm above the sample surface. The time is $t = 20$ s. Inflow is from right to left. The entire width and a portion of the sample length is shown with 1 cm spaced grid lines. The flame shape is presented as the 50 μg/(cm^3 s) reaction rate isosurface (in red). The oxygen mass flux vectors represent the convective only (no diffusion) mass flux of oxygen. This quantity was used in order to mimic, approximately, use of upstream smoke injection for flow visualization, as was done in the experiments of Ref. [10].

used here, heat loss to the ambient gas will eventually extinguish the flame (blowoff) [1].

Effects of Finite Sample Width on Transition to Flame Spread

In Fig. 2, the location of the centerline flame front, as determined by the $Y_C = 0.1$ level of char mass fraction, is plotted versus time as the flame spreads upwind. The trend seen in Fig. 2 is that as the ambient wind speed increased from $u_w = 2$ cm/s to the maximum of $u_w = 10$ cm/s, the flame spread rate increased. This is consistent with earlier experimental and numerical findings [1,3,6]. Also, as the sample width increased from $d = 2$ cm to a maximum of $d = 9$ cm, the spread rate decreased. At early times a clear period of transition (non-monotonic flame spread) existed only for the $u_w = 2$ cm/s cases. The duration of this transition period, from longest to shortest, was approximately 5 s (two-dimensional case), 4 s (three-dimensional, $d = 4$ cm and 9 cm cases), and 3.4 s (three-dimensional, $d = 2$ cm, case); note that radiative flux was turned off at $t = 3.5$ s. Thus, the duration of the transition period increased with sample width when $u_w = 2$ cm/s.

As discussed above, the $u_w = 2$ cm/s cases were in an oxygen-limited environment. This implies that flame transition will be relatively sensitive to changes in the net inflow velocity. Thermal expansion from the flame reduced the ambient wind by an amount ($u_e < 0$) determined by the analytical solution for the potential flow (see equation 2). The net inflow velocity, $u_n = u_w + u_e$, was used in the simulations as the inflow boundary condition in the x-direction (i.e., u_n is the x component of $\underline{u}_{bc}$ in equation 2).

The effects of thermal expansion on the incoming flow have been visualized experimentally using laser-illuminated smoke filaments in flame spread over a liquid pool in microgravity [10]. The convective oxygen mass flux vectors on the bottom half of Fig. 3 show that the incoming flow circumvented the flame in a manner very similar to that seen in Ref. [10]. The incoming flow speed toward the flame front was dramatically reduced (note size of arrowheads) by thermal expansion in both the paper sample holder

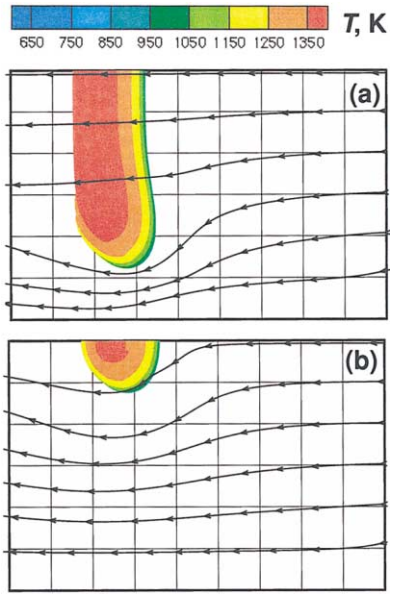

FIG. 4. Top view of both the 9 cm (a) wide and the 2 cm wide (b) samples, with $u_w = 2$ cm/s and paper sample holder. The time is $t = 10$ s. Streamlines are shown. The 50 μg/(cm^3 s) reaction rate isosurface is color contoured with temperature values. The grid in the background is composed of 1 cm spaced lines and does not correspond to the sample boundary except along the upwind edge.

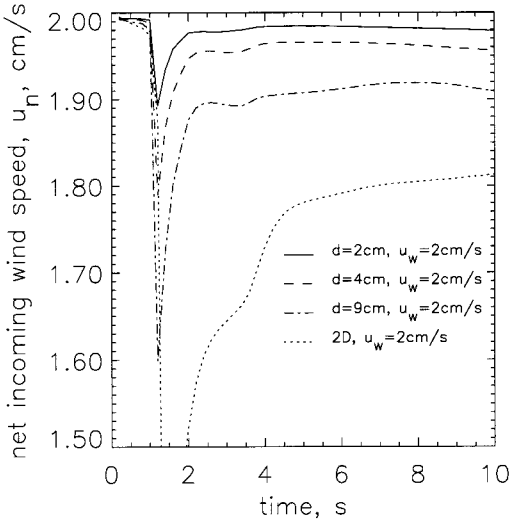

FIG. 5. Net inflow velocity versus time for the three-dimensional simulations of widths $d = 2$ cm, 4 cm, and 9 cm and ambient wind $u_w = 2$ cm/s. The two-dimensional $u_w = 2$ cm/s case is also shown. These values of the inflow velocity are at a specific height ($z = 2.5$ mm) in the free-stream (upwind of the sample) above the centerline in the inflow boundary plane of the simulation. They are characteristic of other vertical locations above the centerline. Rapid, ignition-induced, thermal expansion at early times can be clearly seen in all cases.

case (Fig. 3a) and the steel sample holder case (Fig. 3b). Fig. 4 shows the flowfield environment for the 9 cm wide (Fig. 4a) and the 2 cm wide (Fig. 4b) sample cases. It is clear that in the 2 cm wide sample case, the flame was immersed in a three-dimensional flowfield, even in the centerline region since the streamlines diverged laterally. In the 9 cm wide case, there was very little lateral divergence of the streamlines near the centerline, suggesting that in the centerline area the flow is nearly two-dimensional. The temperatures of the simulated flame seen in Fig. 4 are in the range measured in experiments, 1250 K to 1450 K (thermocouple located 2 mm above the sample surface) [11].

Figure 5 is a plot of the net inflow velocity, u_n, at the centerline versus time for the $u_w = 2$ cm/s, three-dimensional cases with widths $d = 2$ cm, 4 cm, and 9 cm; the two-dimensional case is also shown. The volumetric heat release rate of combustion ($\dot{q}$), which was used in the computation of u_n, was integrated over the flame volume and plotted versus time for the three-dimensional cases in Fig. 6. Here, $\dot{q}$ was determined by summing the product [heat of combustion] $\times$ [local cell volume] $\times$ [reaction rate] for all computational cells in which the reaction rate was greater or equal to 5×10^{-5} g/(cm^3 s). Rapid, ignition-induced heat release began at $t \approx 1$ s and caused a dramatic decrease in the net inflow velocity. This decrease was largest for the widest flame (the two-dimensional case) and smallest for the narrowest flame (2 cm wide three-dimensional flame). After a sufficient time (the transition period), all the flames reached a relatively steady state. Note that the duration of the transition period (in both Fig. 5 and Fig. 2) scales with the how much the ignition event decreased the inflow velocity relative to its ambient value, u_w.

Figure 6 also shows the heat release rate for the three-dimensional, 9 cm wide flames at the higher ambient wind velocities, $u_w = 5$ cm/s and 10 cm/s. The ignition-induced peak heat release rate was nearly identical for all three 9 cm wide cases. For this reason, the ignition-induced expansion velocity was also nearly identical, $u_e \approx -0.4$ cm/s. This was also true for the two-dimensional cases with different u_w (not shown), $u_e \approx -1$ cm/s. Thus, for a given flame width, the ignition-induced u_e is independent of the ambient wind velocity, u_w. This explains why, as u_w increases, the duration of transition decreases. Not only does the oxygen supply improve as u_w increases (making for a more robust flame), but the initial, ignition-induced, expansion-induced velocity is a relatively smaller perturbation from the ambient wind.

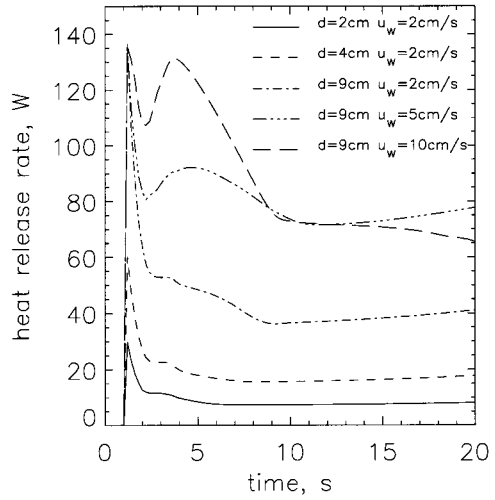

FIG. 6. Heat release rate of gas-phase reaction versus time for all the three-dimensional cases with a stainless steel holder. The heat release rate was found by summing $\dot{q}$ (see equation 2) over all computational cells for which the gas-phase reaction rate was 1 μg/(cm^3 s) or greater.

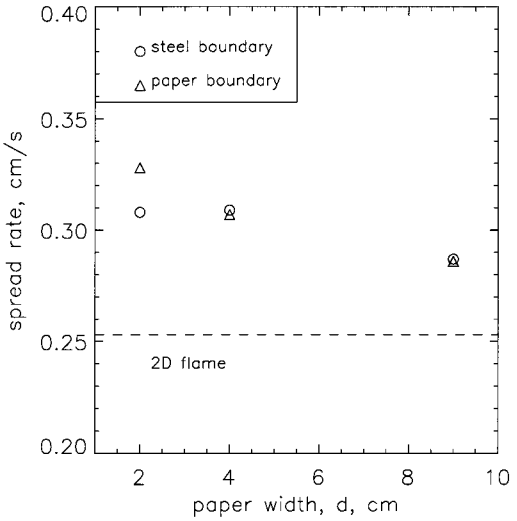

FIG. 7. Upstream centerline flame spread rate versus width, d, of the sample for an ambient wind of u_w = 2 cm/s. Symbols correspond to three-dimensional cases. The case for d = 4 cm with a paper sample holder is not shown. Flame spread rate for two-dimensional case is shown as a dashed line.

There was essentially no difference in the transition behavior of the steel and paper sample holders (u_w = 2 cm/s and d = 2 cm and 9 cm). Differences could have arisen due to greater heat loss to the steel sample holder. Apparently, these effects were not significant during transition. They did, however, influence the post-transition spread rate for the d = 2 cm case, as shown below.

These results show that the sample size has an effect on the duration of the transition period, especially at low ambient wind speeds. Some cases have transition periods that are comparable to the duration of reduced gravity in drop towers. While the results of these simulations have not yet been validated against experimental results, they suggest that choosing a microgravity facility should be done with these issues in mind.

Effects of Finite Sample Width on Established Flame Spread

Flame spread rates were used to investigate the effects of a finite sample width on established flame spread. These were computed by taking the slope of the flame spread curve (e.g., in Fig. 2) over a time interval in which the flame was developing in a relatively steady-state manner. Some care was needed in determining this time interval. The minimum time used was, t_{min} = 5 s, which was after the transition period for all flames (e.g., Fig. 2). The maximum time was chosen to be before the presence of any confounding effects due to proximity to the numerical boundary. Only the fastest traveling flames (the three-dimensional and two-dimensional cases with u_w = 5 cm/s and 10 cm/s) were affected by the numerical boundary (for times greater than approximately 15 s).

Figure 7 shows the flame spread rates, with u_w = 2 cm/s, versus width for the three-dimensional cases. Results for both the steel and paper sample holders are plotted. The spread rate for the two-dimensional case is shown as a dashed line. This figure shows that as the sample width increased, the flame spread rate for both sample holders approached, but did not reach, that of the two-dimensional flame. When d = 2 cm, the flame spread rate was significantly slower for the case of a steel versus a paper sample holder. This implies that relatively large heat losses to the steel sample holder slowed the flame since the spread rates were nearly identical for the widest (d = 9 cm) sample case. This interpretation is corroborated by the fact that flame spread in the d = 4 cm case is as fast as the d = 2 cm case, even though, based on the net inflow velocity in Fig. 5, the d = 2 cm case had a better oxygen supply. Consider also Fig. 3, which shows the temperature of the sample for both the paper (Fig. 3a) and steel (Fig. 3b) sample holder cases. Heat loss effects are clearly greater in Fig. 3b: the flame was smaller, the sample temperature distribution was more confined to the center of the sample, and the peak sample temperature was lower. The distinct difference in the temperature distribution between Fig. 3a and b was due to a relatively strong (hot) flame above the

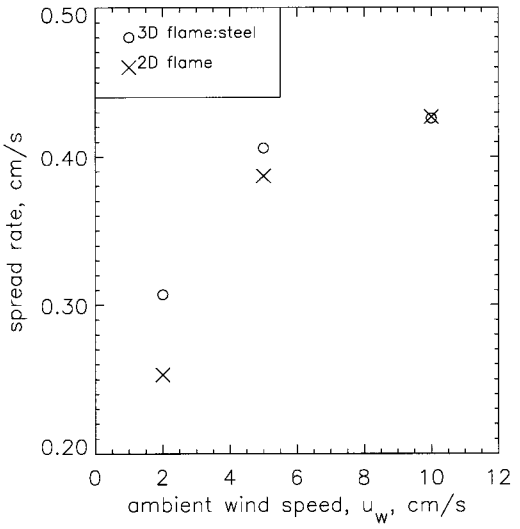

FIG. 8. Upstream centerline flame spread rate versus the ambient wind speed, u_w. Three-dimensional cases with the steel sample holder are shown along with two-dimensional cases.

sample edge in Fig. 3a. The net oxygen mass flux vectors on the upper half of the figures show that this edge flame consumed the oxygen diffusing from the outer free stream before it reached the center. No such edge flame could exist in steel sample case since heat losses at the sample/steel boundary prevented the sample from reaching the pyrolysis temperature. Note that the point of Fig. 7 is that even with a sample sufficiently wide to ensure that edge effects were negligible on the spread rate of the center flame, the spread rate was still not that of the two-dimensional flame.

Figure 8 is a plot of spread rate versus ambient wind speed from the three-dimensional 9 cm wide, steel holder cases and the two-dimensional cases. It is clear that as the ambient wind speed increased, the spread rate of the finite width, 9 cm wide flame tended to the two-dimensional value. This occurred for the same reason the duration of transition decreased as u_w increased: with increased oxygen supply a given width flame was less influenced by other environment factors. For example, the net inflow velocities in the 9 cm three-dimensional and the two-dimensional cases differed by 0.5 cm/s (not shown) when $u_w = 10$ cm/s. This is 5 times their difference when $u_w = 2$ cm/s (see Fig. 5). But three- and two-dimensional flame spreads agreed when $u_w = 10$ cm/s because there was an abundance of oxygen. This can easily be seen in Fig. 8 by the relative insensitivity of the flame spread rate to changes in u_w (i.e., the formation of a plateau) as u_w increases. Although the simulations were not performed, it is possible that even for the 2 cm sample width, the three- and two-dimensional flame spread rates would be in better agreement as u_w increased.

Conclusions

The width of the sample affected both the duration of the flame transition period and the post-transition flame spread rate. Finite width affects were most significant when the ambient wind was relatively small (limited oxygen supply). In such environments, the velocity due to thermal expansion from the flame reduced the net inflow of oxygen enough to significantly affect flame behavior. The expansion velocity increased with increasing flame size (i.e., sample width). For a given sample width, the influence of thermal expansion on the net incoming oxygen supply decreased as the ambient wind speed increased. Thus, both the transition and flame spread behavior of the three-dimensional flame (along the centerline) tended to that of the two-dimensional flame with increasing ambient wind speed. These results emphasize the importance of including velocity boundary conditions which account for thermal expansion effects at low ambient wind velocities.

Heat losses to the sample holder were found to significantly lower the temperature on the sample near the sample–sample holder interface. As a result, the flame spread rate in the case of the narrowest sample, with the slowest ambient wind, was reduced. These results are based on simulations only. Further microgravity experiments are needed to conclusively validate these findings.

Acknowledgments

This work is funded by the NASA Microgravity Science Program under the Inter-Agency Agreement no. C-32001-R under technical monitor Dr. Sandra Olson.

REFERENCES

1. Olson, S. L., *Combust. Sci. Technol.* 76:233–249 (1991).
2. Grayson, G. D., Sacksteader, K., Ferkeul, P. V., and T'ien, J. S., *Microgravity Sci. Technol.* 99:345–370 (1994).
3. McGrattan, K. B., Kashiwagi, T., Baum, H. R., and Olson, S. L., *Combust. Flame* 106:377–391 (1996).
4. Bhattacharjee, S., Altenkirch, R. A., and Sacksteader, K., *Combust. Sci. Technol.* 91:225–242 (1993).
5. Altenkirch, R. A., Tang, L., Sacksteader, K., Bhattacharjee, S., and Delichatsios, M. A., *Proc. Combust. Inst.* 27:2515–2524 (1998).
6. Mell, W. E., and Kashiwagi, T., *Proc. Combust. Inst.* 27:2635–2641 (1998).

7. Kashiwagi, T., and Nambu, H., *Combust. Flame* 88:345–368 (1992).
8. Nakabe, K., McGrattan, K. B., Kashiwagi, T., Baum, H. R., Yamashita, H., and Kushida, G., *Combust. Flame* 98:361–374 (1994).
9. Kashiwagi, T., McGrattan, K. B., Olson, S. L., Fujita, O., Kikuchi, M., and Ito, K., *Proc. Combust. Inst.* 26:1345–1352 (1996).
10. Miller, F. J., and Ross, H. D., *Proc. Combust. Inst.* 27:2715–2722 (1998).
11. Olson, S. L., Kashiwagi, T., Fujita, O., Kikuchi, M., and Ito, K., "Experimental Observation of Spot Radiative Ignition and Subsequent Three-Dimensional Flame Spread Over Thin Cellulose Fuels" *Combust. Flame* in press.